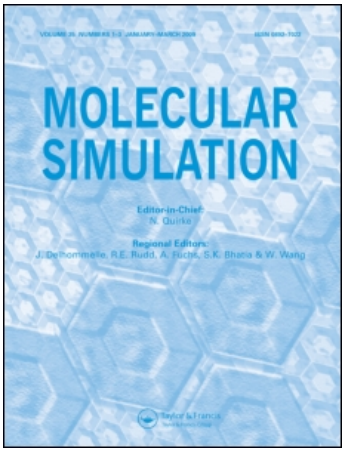

Molecular Simulation
Publication details, including instructions for authors and subscription information:
http://www.informaworld.com/smpp/title~content=t713644482

Solution Microstructure of Confined Fluids with Directional Interactions under the Influence of an External Field: Mean Field Considerations

J. S. Erickson[a]; G. L. Aranovich[a]; M. D. Donohue[a]
[a] Johns Hopkins University, Baltimore, MD, USA

To cite this Article Erickson, J. S. , Aranovich, G. L. and Donohue, M. D.(2004) 'Solution Microstructure of Confined Fluids with Directional Interactions under the Influence of an External Field: Mean Field Considerations', Molecular Simulation, 30: 8, 507 — 520
To link to this Article: DOI: 10.1080/08927020410001667557
URL: http://dx.doi.org/10.1080/08927020410001667557

Molecular Simulation, Vol. 30 (8), 15 July 2004, pp. 507–520

Taylor & Francis
Taylor & Francis Group

Solution Microstructure of Confined Fluids with Directional Interactions under the Influence of an External Field: Mean Field Considerations

J.S. ERICKSON*, G.L. ARANOVICH and M.D. DONOHUE

Johns Hopkins University, 3400 N. Charles Street, Baltimore, MD 21218, USA

(Received September 2003; In final form January 2004)

Lattice density functional theory (DFT) and Monte Carlo simulations are used to probe the phase behavior and equilibrium structure of molecules with directional interactions with and without the influence of body forces. It is found that the application of a position-specific external field can be used to control the microstructure of confined fluids. In the absence of an external field, a condensation transition can take place within the pore at sufficiently high densities. This phase transition results in a solution microstructure made up of chains of monomers oriented parallel to the pore walls. With the application of a weak field, it is possible to disrupt this solution microstructure. This type of effect could allow controlled mixing at a local level. Upon application of a stronger field, chains reform in a direction perpendicular to the walls.

Keywords: Adsorption; Monte Carlo; Density functional theory; Phase transition; External field

INTRODUCTION

Solutions made up of molecules with directionally dependent interaction potentials are important in a large number of fields. Perhaps the most common example of such a fluid is water. The ability of water to form directionally specific hydrogen bonds profoundly affects its thermodynamic and solvent properties [1]. As a liquid, water forms three-dimensional network structures. These hydrogen bonds become even more dominant in ice, resulting in an open, cage-like microstructure and an expansion upon freezing. Additionally, it is believed that directional interactions are responsible for an order-disorder phase transition in the hydrogen bond network of supercooled water with a critical point at roughly -45°C, just below the experimental limit of attainable supercooling in liquid water [1–3].

There are many other examples of systems where directional interactions are important. In living polymers, monomers react reversibly to form chains [4,5]. Molecules of this type include bio-polymers such as actin [5], tubulin [6], and the tobacco mosaic virus [7], as well as inorganic molecules such as sulfur [5]. Fibrinogen [8,9] is very similar to a living polymer because nucleation and growth steps are involved and directional interactions determine the resulting network structure, although the bond formation is irreversible. In hydrogen fluoride, directionally specific hydrogen bonding is responsible for the formation of long, one-dimensional networks of molecules in the shape of winding chains in the liquid state [10]. Magnetic materials also have directional interactions and can exhibit the same kinds of phenomena described in this work [11].

Although molecules with directional interactions are commonly found in nature, general theories are unable to account for the unusual thermodynamic behavior that these systems exhibit. In order to get accurate predictions, it has been found that either the directional interactions must be taken into account specifically, or else the resulting clusters that are formed must be treated explicitly. Several different classical and molecular thermodynamic techniques have been developed to do this. The earliest approaches to model the thermodynamic behavior of fluids with directional interactions used either chemical or quasi-chemical theory. In chemical theory [12],

*Corresponding author. E-mail: mdd@jhu.edu

ISSN 0892-7022 print/ISSN 1029-0435 online © 2004 Taylor & Francis Ltd
DOI: 10.1080/08927020410001667557

clusters of molecules are treated as distinct species in dynamic equilibrium with each other. Such an approach has been applied successfully to molecules that form small clusters (e.g. dimers). However, chemical theory becomes cumbersome when the formation of large networks or clusters must be considered, because each distinct "species" requires the specification of an equilibrium constant [13]. By contrast, quasi-chemical theory [14] postulates that non-idealities in solutions can be related to non-random mixing on the local level. Such an approach is usually associated with lattice theory. In these theories, the formation of distinct networks or clusters is not considered, but instead the (isotropic) intermolecular interaction energy is increased in order to duplicate non-ideal behavior seen on the macroscopic level. The use of chemical and quasi-chemical methods for modeling fluids with directional interactions has been reviewed by Economou *et al.* [15].

More recently, several molecular thermodynamic approaches have been developed to model associating fluids, including decorated Ising models [16–19], Monte Carlo [20,21] and molecular dynamics simulations [22], the associated perturbed anisotropic chain theory (APACT) [23], and the statistical associating fluid theory (SAFT) [13,24]. Decorated Ising models are lattice models that allow for the exact solutions of the phase behavior and thermodynamic properties of molecules with directional interactions in two dimensions, and excellent approximations in three dimensions. However, in these theories, the locations of the molecules are limited to arrangements that can be mathematically mapped onto the standard Ising model, effectively restricting their use. APACT and SAFT are off-lattice theories that have been shown to give excellent approximations for the behavior of associating fluids. In contrast to the previous models, both of these approaches are based on the use of thermodynamic perturbation theory. In order to include realistic assumptions about the intermolecular interaction potentials and location of the interaction sites, the equations become mathematically complex [25]. Such difficulties can be avoided by the use of Monte Carlo and molecular dynamics simulations. Although these techniques are accurate, they tend to be time consuming to execute.

In this work, molecules with directional interactions are modeled using a different approach, lattice density functional theory (DFT) [26]. This approach is a mean field theory, and it takes advantage of the mathematical simplicity inherent in lattice theories, but is not limited to isotropic interactions or specific geometries as quasi-chemical theory and decorated Ising models are. Mean field theories are generally known to be accurate beyond the critical regions of the phase diagram, and have been important in the development of models that consider crossover behavior from classical to critical [27–29]. Furthermore, mean field theories have been successfully used for the generation of qualitatively correct phase diagrams such as those for polymers [30] and for wetting and prewetting transitions [31].

Although most applications of lattice DFT have been for modeling the adsorption of molecules with isotropic interaction potentials, a few studies have considered molecules with directional interactions. In Aranovich *et al.* [32], monomers with directional interactions were studied in bulk solution. That study was recently extended to include adsorbed and confined fluids [33]. In this work, we continue to build on these previous studies by considering the effect of an applied external field.

In contrast to isotropic monomers, molecules with directional interactions have distinguishable orientations. For this reason, they can form molecular or supramolecular structures such as chains or clusters of molecules with a specific configuration. It has been shown that by specifying short ranged potentials between molecules or between a molecule and a surface, the formation of such structures can be controlled [33]. These short ranged interactions propagate into the fluid and cause large changes in solution microstructure throughout a pore or film. Generally, relatively strong molecular interactions are required to observe such an effect. It may be possible generate the same types of ordered structures with a much weaker, locally-applied external field. It is the goal of this study to examine the effect of such a field on the formation of ordered structures.

THEORY

Model

In this study, molecules with directional interactions are modeled in two dimensions as monomers on a square lattice confined within a slit-like pore. These monomers have *A*-sides and *B*-sides, as depicted in Fig. 1. Because of the directional

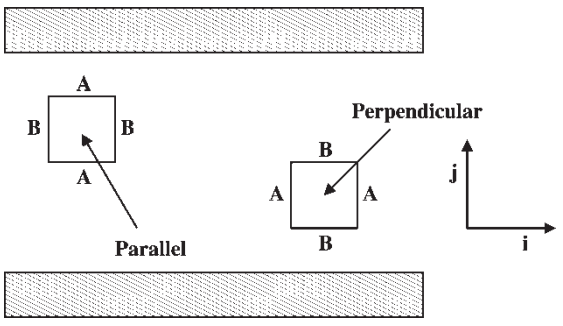

FIGURE 1 A typical pore. A parallel and a perpendicular monomer are shown inside the pore. Parallel monomers are defined as having their *A*-sides pointing towards the walls. Perpendicular monomers have their *B*-sides oriented towards the walls.

interactions present in the system, two distinct orientations of monomers are possible. These orientations are described as parallel (*A*-sides pointing towards the surface) and perpendicular (*B*-sides oriented towards the surface). Monomers are assumed to interact with nearest neighbor $A-A$, $A-B$, and $B-B$ molecule–molecule interactions, and $A-S$ and $B-S$ molecule–surface interactions. Furthermore, an external field can be imposed upon all monomers within the pore. The effect of the field is to favor monomers in the perpendicular orientation. In this work, the external field is considered to be a function of the distance along the pore, which is explicitly stated as $\varepsilon_{\text{field}}(i)$.

Let $x_{\parallel,i,j}$ represent the concentration of molecules in the parallel orientation, $x_{\perp,i,j}$ the density of molecules in the perpendicular orientation, and x_∞ the density of molecules in a hypothetical bulk reservoir. Then the total density of molecules at each lattice site is given by

$$x_{ij} = x_{\parallel,i,j} + x_{\perp,i,j} \tag{1}$$

Because there is an equal probability of finding a monomer in the parallel or perpendicular configuration in the bulk reservoir, it follows that

$$x_{\parallel,\infty} = x_{\perp,\infty} = \frac{x_\infty}{2} \tag{2}$$

Lattice DFT

In order to find the equilibrium monomer densities in the pore, the free energy A, of the system is minimized using the principles of lattice DFT [34,35]

$$A[\rho(i,j)] = U - TS \rightarrow \text{minimum} \tag{3}$$

Here, A is a function of the density distribution $\rho(i,j)$. In the mean field approximation [36], the average energy and entropy at any site in the lattice can be written as

$$\begin{aligned} U = {} & x_{\parallel,i,j}(x_{\parallel,i+1,j}\varepsilon_{BB} + x_{\parallel,i,j+1}\varepsilon_{AA} + x_{\parallel,i-1,j}\varepsilon_{BB} + x_{\parallel,i,j-1}\varepsilon_{AA}) \\ & + x_{\parallel,i,j}(x_{\perp,i+1,j} + x_{\perp,i,j+1} + x_{\perp,i-1,j} + x_{\perp,i,j-1})\varepsilon_{AB} \\ & + x_{\perp,i,j}(x_{\parallel,i+1,j} + x_{\parallel,i,j+1} + x_{\parallel,i-1,j} + x_{\parallel,i,j-1})\varepsilon_{AB} \\ & + x_{\perp,i,j}(x_{\perp,i+1,j}\varepsilon_{AA} + x_{\perp,i,j+1}\varepsilon_{BB} + x_{\perp,i-1,j}\varepsilon_{AA} \\ & + x_{\perp,i,j-1}\varepsilon_{BB}) + x_{\perp,i,j}\varepsilon_{\text{field}}(i) \end{aligned} \tag{4}$$

and

$$\begin{aligned} S = {} & -k(x_{\parallel,i,j}\ln x_{\parallel,i,j} + x_{\perp,i,j}\ln x_{\perp,i,j} \\ & + [1 - x_{\parallel,i,j} - x_{\perp,i,j}]\ln[1 - x_{\parallel,i,j} - x_{\perp,i,j}]) \end{aligned} \tag{5}$$

The free energy is then minimized by the method of Lagrange multipliers [37], subject to the constraint

$$\phi = \sum_i \sum_j [x_{\parallel,i,j} + x_{\perp,i,j}] = \alpha_M \tag{6}$$

where α_M is the overall number of molecules in the system. To proceed, one first constructs the function

$$\Omega = A - \mu\phi \tag{7}$$

where μ is a Lagrange multiplier. Next, derivatives

$$\frac{\partial \Omega}{\partial x_{\parallel,i,j}} = 0 \tag{8}$$

and

$$\frac{\partial \Omega}{\partial x_{\perp,i,j}} = 0 \tag{9}$$

are calculated. In expressions (8) and (9), the quantity $\partial\phi/\partial x_k$ is equal to 1, so that the Lagrange multiplier μ reduces to $\partial A/\partial x_k$ with temperature, volume, and all monomer species except k being held fixed. This shows that the Lagrange multipliers can be identified with the chemical potential of each species of monomer at each site on the lattice. Combining Eqs. (3)–(7) and taking derivatives (8) and (9) leads to the following expressions for the Lagrange multipliers

$$\begin{aligned} \mu_{\parallel,i,j} = {} & kT\ln\left(\frac{x_{\parallel,i,j}}{1 - x_{\parallel,i,j} - x_{\perp,i,j}}\right) + x_{\parallel,i+1,j}\varepsilon_{BB} + x_{\parallel,i,j+1}\varepsilon_{AA} \\ & + x_{\parallel,i-1,j}\varepsilon_{BB} + x_{\parallel,i,j-1}\varepsilon_{AA} + x_{\perp,i+1,j}\varepsilon_{AB} \\ & + x_{\perp,i,j+1}\varepsilon_{AB} + x_{\perp,i-1,j}\varepsilon_{AB} + x_{\perp,i,j-1}\varepsilon_{AB} \end{aligned} \tag{10}$$

and

$$\begin{aligned} \mu_{\perp,i,j} = {} & kT\ln\left(\frac{x_{\perp,i,j}}{1 - x_{\parallel,i,j} - x_{\perp,i,j}}\right) + x_{\perp,i+1,j}\varepsilon_{AA} \\ & + x_{\perp,i,j+1}\varepsilon_{BB} + x_{\perp,i-1,j}\varepsilon_{AA} + x_{\perp,i,j-1}\varepsilon_{BB} \\ & + x_{\parallel,i+1,j}\varepsilon_{AB} + x_{\parallel,i,j+1}\varepsilon_{AB} \\ & + x_{\parallel,i-1,j}\varepsilon_{AB} + x_{\parallel,i,j-1}\varepsilon_{AB} + \varepsilon_{\text{field}}(i) \end{aligned} \tag{11}$$

At layers bordering the walls ($j = 1$ and $j = N$), slightly modified equations are obtained. These equations take into account the interaction of a molecule with the surface, and are given by

$$\begin{aligned} \mu_{\parallel,i,j} = {} & kT\ln\left(\frac{x_{\parallel,i,1}}{1 - x_{\parallel,i,1} - x_{\perp,i,1}}\right) + x_{\parallel,i+1,1}\varepsilon_{BB} \\ & + x_{\parallel,i,2}\varepsilon_{AA} + x_{\parallel,i-1,1}\varepsilon_{BB} + x_{\perp,i+1,1}\varepsilon_{AB} \\ & + x_{\perp,i,2}\varepsilon_{AB} + x_{\perp,i-1,1}\varepsilon_{AB} + \varepsilon_{AS} \end{aligned} \tag{12}$$

and

$$\mu_{\perp,i,j} = kT\ln\left(\frac{x_{\perp,i,1}}{1-x_{\parallel,i,1}-x_{\perp,i,1}}\right) + x_{\perp,i+1,1}\varepsilon_{AA} + x_{\perp,i,2}\varepsilon_{BB} + x_{\perp,i-1,1}\varepsilon_{AA} + x_{\parallel,i+1,1}\varepsilon_{AB} + x_{\parallel,i,2}\varepsilon_{AB} + x_{\parallel,i-1,1}\varepsilon_{AB} + \varepsilon_{BS} + \varepsilon_{\text{field}}(i) \quad (13)$$

for $j=1$ and

$$\mu_{\parallel,i,j} = kT\ln\left(\frac{x_{\parallel,i,N}}{1-x_{\parallel,i,N}-x_{\perp,i,N}}\right) + x_{\parallel,i+1,N}\varepsilon_{BB} + x_{\parallel,i,N-1}\varepsilon_{AA} + x_{\parallel,i-1,N}\varepsilon_{BB} + x_{\perp,i+1,N}\varepsilon_{AB} + x_{\perp,i,N-1}\varepsilon_{AB} + x_{\perp,i-1,N}\varepsilon_{AB} + \varepsilon_{AS} \quad (14)$$

and

$$\mu_{\perp,i,j} = kT\ln\left(\frac{x_{\perp,i,N}}{1-x_{\parallel,i,N}-x_{\perp,i,N}}\right) + x_{\perp,i+1,N}\varepsilon_{AA} + x_{\perp,i,N-1}\varepsilon_{BB} + x_{\perp,i-1,N}\varepsilon_{AA} + x_{\parallel,i+1,N}\varepsilon_{AB} + x_{\parallel,i,N-1}\varepsilon_{AB} + x_{\parallel,i-1,N}\varepsilon_{AB} + \varepsilon_{BS} + \varepsilon_{\text{field}}(i) \quad (15)$$

for $j=N$.

Assuming that there is no external field in the bulk reservoir, an additional constraint can be obtained from Eqs. (2),(10) or (11)

$$\mu_\infty = kT\ln\left(\frac{x_\infty/2}{1-x_\infty}\right) + x_\infty\varepsilon_{AA} + x_\infty\varepsilon_{BB} + 2x_\infty\varepsilon_{AB} \quad (16)$$

In order to obtain equations for the density distribution of the fluid inside the pore, chemical potentials (10)–(16) are set equal to each other. This leads to equations for the adsorption isotherms such as

$$\ln\left[\frac{x_{\parallel,i,j}(1-x_\infty)}{\frac{x_\infty}{2}(1-x_{\parallel,i,j}-x_{\perp,i,j})}\right] + x_{\parallel,i+1,j}\frac{\varepsilon_{BB}}{kT} + x_{\parallel,i,j+1}\frac{\varepsilon_{AA}}{kT} + x_{\parallel,i-1,j}\frac{\varepsilon_{BB}}{kT} + x_{\parallel,i,j-1}\frac{\varepsilon_{AA}}{kT} + \left(x_{\perp,i+1,j} + x_{\perp,i,j+1} + x_{\perp,i-1,j} + x_{\perp,i,j-1}\right)\frac{\varepsilon_{AB}}{kT} = x_\infty\left(\frac{\varepsilon_{AA}}{kT} + \frac{\varepsilon_{BB}}{kT} + 2\frac{\varepsilon_{AB}}{kT}\right)$$

from Eqs. (10) and (16), and

$$\ln\left[\frac{x_{\perp,i,j}(1-x_\infty)}{\frac{x_\infty}{2}(1-x_{\parallel,i,j}-x_{\perp,i,j})}\right] + (x_{\parallel,i+1,j} + x_{\parallel,i,j+1} + x_{\parallel,i-1,j} + x_{\parallel,i,j-1})\frac{\varepsilon_{AB}}{kT} + x_{\perp,i+1,j}\frac{\varepsilon_{AA}}{kT} + x_{\perp,i,j+1}\frac{\varepsilon_{BB}}{kT} + x_{\perp,i-1,j}\frac{\varepsilon_{AA}}{kT} + x_{\perp,i,j-1}\frac{\varepsilon_{BB}}{kT} + \frac{\varepsilon_{\text{field}}(i)}{kT} = x_\infty\left(\frac{\varepsilon_{AA}}{kT} + \frac{\varepsilon_{BB}}{kT} + 2\frac{\varepsilon_{AB}}{kT}\right)$$

from Eqs. (11) and (16). After some manipulations, one obtains

$$x_{\parallel,i,j} = \frac{x_\infty(1-x_{\perp,i,j})}{x_\infty + 2(1-x_\infty)\exp\left(\frac{\varepsilon_1^*}{kT}\right)} \quad (17)$$

and

$$x_{\perp,i,j} = \frac{x_\infty(1-x_{\parallel,i,j})}{x_\infty + 2(1-x_\infty)\exp\left(\frac{\varepsilon_2^*}{kT}\right)} \quad (18)$$

where

$$\varepsilon_1^* = x_{\parallel,i+1,j}\varepsilon_{BB} + x_{\parallel,i,j+1}\varepsilon_{AA} + x_{\parallel,i-1,j}\varepsilon_{BB} + x_{\parallel,i,j-1}\varepsilon_{AA} + x_{\perp,i+1,j}\varepsilon_{AB} + x_{\perp,i,j+1}\varepsilon_{AB} + x_{\perp,i-1,j}\varepsilon_{AB} + x_{\perp,i,j-1}\varepsilon_{AB} \quad (19)$$

and

$$\varepsilon_2^* = x_{\parallel,i+1,j}\varepsilon_{AB} + x_{\parallel,i,j+1}\varepsilon_{AB} + x_{\parallel,i-1,j}\varepsilon_{AB} + x_{\parallel,i,j-1}\varepsilon_{AB} + x_{\perp,i+1,j}\varepsilon_{AA} + x_{\perp,i,j+1}\varepsilon_{BB} + x_{\perp,i-1,j}\varepsilon_{AA} + x_{\perp,i,j-1}\varepsilon_{BB} + \varepsilon_{\text{field}}(i) \quad (20)$$

when $j \neq 1$ or N, along with j-direction boundary conditions

$$\varepsilon_1^* = x_{\parallel,i+1,1}\varepsilon_{BB} + x_{\parallel,i,2}\varepsilon_{AA} + x_{\parallel,i-1,1}\varepsilon_{BB} + x_{\perp,i+1,1}\varepsilon_{AB} + x_{\perp,i,2}\varepsilon_{AB} + x_{\perp,i-1,1}\varepsilon_{AB} + \varepsilon_{AS} \quad (21)$$

and

$$\varepsilon_2^* = x_{\parallel,i+1,1}\varepsilon_{AB} + x_{\parallel,i,2}\varepsilon_{AB} + x_{\parallel,i-1,1}\varepsilon_{AB} + x_{\perp,i+1,1}\varepsilon_{AA} + x_{\perp,i,2}\varepsilon_{BB} + x_{\perp,i-1,1}\varepsilon_{AA} + \varepsilon_{BS} + \varepsilon_{\text{field}}(i) \quad (22)$$

for $j=1$, and

$$\varepsilon_1^* = x_{\parallel,i+1,N}\varepsilon_{BB} + x_{\parallel,i,N-1}\varepsilon_{AA} + x_{\parallel,i-1,N}\varepsilon_{BB} + x_{\perp,i+1,N}\varepsilon_{AB} + x_{\perp,i,N-1}\varepsilon_{AB} + x_{\perp,i-1,N}\varepsilon_{AB} + \varepsilon_{AS} \quad (23)$$

and

$$\varepsilon_2^* = x_{\parallel,i+1,N}\varepsilon_{AB} + x_{\parallel,i,N-1}\varepsilon_{AB} + x_{\parallel,i-1,N}\varepsilon_{AB} + x_{\perp,i+1,N}\varepsilon_{AA} + x_{\perp,i,N-1}\varepsilon_{BB} + x_{\perp,i-1,N}\varepsilon_{AA} + \varepsilon_{BS} + \varepsilon_{\text{field}}(i) \quad (24)$$

for $j = \text{N}$.

Finally, it is necessary to formulate boundary conditions in the i-direction. In this work it is assumed that the pore is infinite in length, so that there are no edge effects to consider. As there are no walls in the i-direction to bound the pore and the external field $\varepsilon_{\text{field}}(i)$ is assumed to be non-uniform, it is necessary to have some knowledge about the shape of the field before these boundary conditions can be specified. In this work, a Gaussian shape is used for the applied external field. The general shape of this field is illustrated in Fig. 2. The field starts at zero, increases in a Gaussian manner to a maximum value, remains there for a specified distance sigma, and then weakens in a Gaussian manner back to zero. Because the field is non-zero only in a finite region of the pore, the effects of the applied field on the fluid must decay to zero at some distance into the region where the field is absent. Therefore, far from this non-zero region, it is assumed that

$$x_{\parallel,i+1,j} = x_{\parallel,i,j} \quad (25)$$

and

$$x_{\perp,i+1,j} = x_{\perp,i,j} \quad (26)$$

These conditions are applied to Eqs. (19)–(24), depending on whether the j-layer is next to a wall or not. For the case when $i = 1$, this leads to six additional expressions

$$\varepsilon_1^* = x_{\parallel,1,j}\varepsilon_{BB} + x_{\parallel,2,j}\varepsilon_{BB} + x_{\parallel,1,j+1}\varepsilon_{AA} + x_{\parallel,1,j-1}\varepsilon_{AA} + x_{\perp,1,j}\varepsilon_{AB} + x_{\perp,2,j}\varepsilon_{AB} + x_{\perp,1,j+1}\varepsilon_{AB} + x_{\perp,1,j-1}\varepsilon_{AB} \quad (27)$$

and

$$\varepsilon_2^* = x_{\parallel,1,j}\varepsilon_{AB} + x_{\parallel,2,j}\varepsilon_{AB} + x_{\parallel,1,j+1}\varepsilon_{AB} + x_{\parallel,1,j-1}\varepsilon_{AB} + x_{\perp,1,j}\varepsilon_{AA} + x_{\perp,2,j}\varepsilon_{AA} + x_{\perp,1,j+1}\varepsilon_{BB} + x_{\perp,1,j-1}\varepsilon_{BB} \quad (28)$$

when $j \neq 1$ or N,

$$\varepsilon_1^* = x_{\parallel,1,1}\varepsilon_{BB} + x_{\parallel,2,1}\varepsilon_{BB} + x_{\parallel,1,2}\varepsilon_{AA} + x_{\perp,1,1}\varepsilon_{AB} + x_{\perp,2,1}\varepsilon_{AB} + x_{\perp,1,2}\varepsilon_{AB} + \varepsilon_{AS} \quad (29)$$

and

$$\varepsilon_2^* = x_{\parallel,1,1}\varepsilon_{AB} + x_{\parallel,2,1}\varepsilon_{AB} + x_{\parallel,1,2}\varepsilon_{AB} + x_{\perp,1,1}\varepsilon_{AA} + x_{\perp,2,1}\varepsilon_{AA} + x_{\perp,1,2}\varepsilon_{BB} + \varepsilon_{BS} \quad (30)$$

when $j = 1$, and

$$\varepsilon_1^* = x_{\parallel,1,N}\varepsilon_{BB} + x_{\parallel,2,N}\varepsilon_{BB} + x_{\parallel,1,N-1}\varepsilon_{AA} + x_{\perp,1,N}\varepsilon_{AB} + x_{\perp,2,N}\varepsilon_{AB} + x_{\perp,1,N-1}\varepsilon_{AB} + \varepsilon_{AS} \quad (31)$$

and

$$\varepsilon_2^* = x_{\parallel,1,N}\varepsilon_{AB} + x_{\parallel,2,N}\varepsilon_{AB} + x_{\parallel,1,N-1}\varepsilon_{AB} + x_{\perp,1,N}\varepsilon_{AA} + x_{\perp,2,N}\varepsilon_{AA} + x_{\perp,1,N-1}\varepsilon_{BB} + \varepsilon_{BS} \quad (32)$$

when $j = N$. The fact that $\varepsilon_{\text{field}}(1) = 0$ has been included in these expressions. Boundary conditions on the other side of the field also exist; these are obtained by replacing $i = 1$ and $i = 2$ with $i = M$ and $i = (M - 1)$ in Eqs. (27)–(32), where M is the last layer considered in the i-direction.

The location of the boundary conditions in the i-direction must be chosen with care. In this work, calculations were repeated with the i-direction boundary conditions at several different distances away from the region where the applied external field was zero. When the results of the calculation no

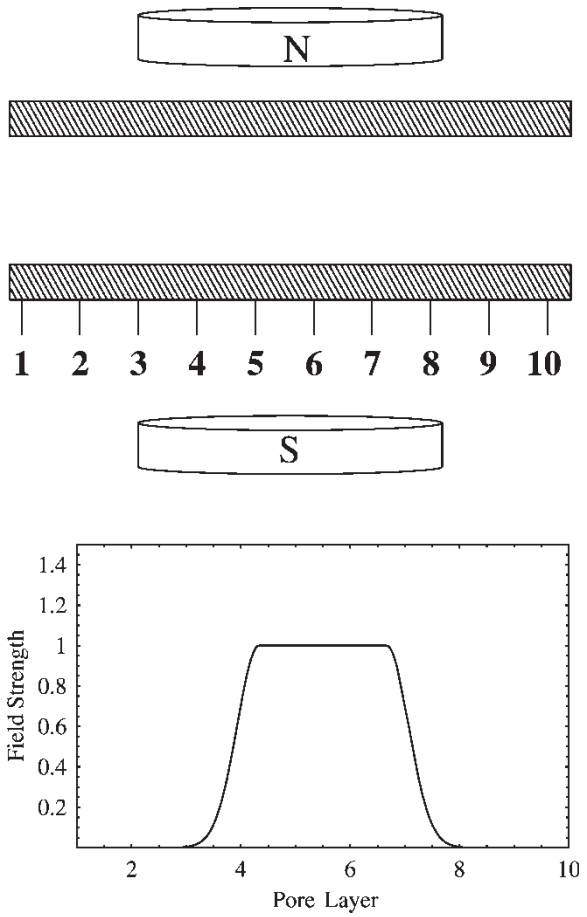

FIGURE 2 (a) A sketch of a ten layer pore with an external field that affects layers 4–7. (b) The shape of the locally applied external field. The field strength has units of ε/kT.

longer changed as this distance was increased, it was assumed that the effects of the field propagating into the region of the fluid where the field was zero had died off.

The Eqs. (17) and (18), with conditions (19)–(24) and (27)–(32), were solved iteratively by the method of successive substitutions to determine the equilibrium monomer density at each site in the lattice. In these calculations, the adsorbed density is calculated as a function of layer number in the *i*-direction, which is the direction in which the external field varies. The adsorbed density is averaged over all layers in the *j*-direction, which is the direction perpendicular to the walls.

The calculations in this study were performed in two dimensions. However, it is possible to generalize such an approach to three dimensions. In the case of a pore that does not vary in its third dimension, such as the slit-like pores in graphite, the results of this study are relevant and can be directly extended. Pores that have an irregular, three-dimensional structure can also be modeled using lattice DFT, provided that appropriate boundary conditions are chosen. Finally, it is noted that it is also possible to generalize this approach to molecules of irregular size or shape; as an example, the adsorption of dimers was modeled using lattice DFT by Wu *et al.* [38].

Gibbs Integral Equation

In order to construct a phase diagram, knowledge of the binodal points is necessary. These points can be found from the requirements that coexisting phases exhibit equal temperatures, pressures and chemical potentials. Since lattice DFT is constructed in the grand ensemble, the temperatures and chemical potentials of any coexisting phases are already equal. Therefore, in order to find the binodal points, the condition of equal pressures must be enforced. The procedure for determining the coexistence pressure is known as the Gibbs integral construction [39], and has been done previously by Aranovich *et al.* [35] for isotropic monomers where the adsorption isotherm was obtained by a solution technique that explicitly predicted points in the unphysical region. In this work, the lattice DFT equations are solved by the method of successive substitutions, which give no points in the unphysical region of the isotherm. Furthermore, the monomers in this work have directional interactions. Therefore, an outline of the derivation for the Gibbs integral equation is given here.

In order to construct an equation to predict the location of the binodal points, one begins with the Gibbs adsorption equation for a two component system

$$-\mathrm{d}\gamma = \mathrm{d}\sigma = \Gamma_A \mathrm{d}\mu_A + \Gamma_B \mathrm{d}\mu_B = \Gamma_A \mathrm{d}(\mu_A - \mu_B)$$

where γ is the surface tension, σ is the surface pressure, Γ_A is the Gibbs excess of component A at the interface, and μ_A is the chemical potential of component A. To continue, it is noted that lattice DFT requires the parallel, perpendicular and bulk monomers to have the same chemical potential. Then component A can be identified as the monomers, and component B as the holes. Since the lattice DFT expressions for chemical potential are relative to the concentration of holes, an expression for $(\mu_A - \mu_B)$ is given by Eq. (16)

$$\mu_\infty = (\mu_A - \mu_B) = kT \ln\left(\frac{x_\infty/2}{1 - x_\infty}\right) + x_\infty(\varepsilon_{AA} + \varepsilon_{BB} + 2\varepsilon_{AB})$$

Then

$$\frac{\mathrm{d}(\mu_A - \mu_B)}{\mathrm{d}x_\infty} = \frac{kT}{x_\infty(1 - x_\infty)} + (\varepsilon_{AA} + \varepsilon_{BB} + 2\varepsilon_{AB}) = \frac{\mathrm{d}\sigma}{\mathrm{d}x_\infty}\frac{1}{\Gamma_A}$$

Finally, one can integrate to arrive at the expression

$$\frac{\sigma}{kT} = \int_0^{x_\infty} \frac{\Gamma_A\left[1 + x_\infty(1 - x_\infty)(\varepsilon_{AA} + \varepsilon_{BB} + 2\varepsilon_{AB})\right]}{x_\infty(1 - x_\infty)}\mathrm{d}x_\infty \tag{33}$$

This equation was used to find the coexistence pressure from adsorption isotherms calculated by the method of successive substitutions. Once the coexistence pressure was known, the binodal points could be read from the adsorption isotherms by inspection.

The procedure for numerically integrating Eq. (33) was slightly tricky. As shown in Fig. 3a, data obtained by successive substitutions gives no information about the unphysical region of the isotherm. In order to perform the integration, information needed to be assumed for this region. In this work, a linear function was chosen to interpolate between the spinodal points, which are shown as the large dots in Fig. 3a. The dashed line in Fig. 3b is the region of the Gibbs integral construction that results from the unphysical part of the isotherm. It is expected that the choice of interpolating function will not have a large effect on the location at which the lines cross, and therefore should not affect the coexistence pressure.

Grand Canonical Ensemble Monte Carlo

In order to test the theory, lattice Monte Carlo simulations were performed in the grand canonical ensemble [40,41]. For molecules confined within

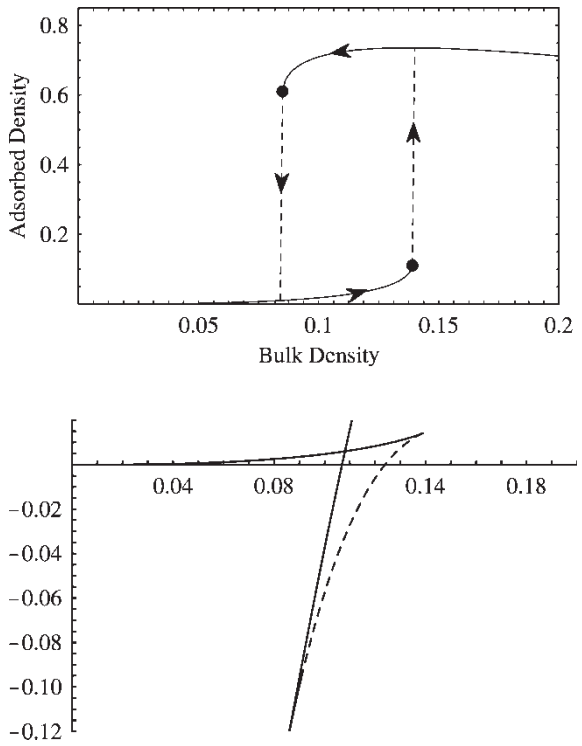

FIGURE 3 Data obtained in the phase coexistence region from lattice DFT by the method of successive substitutions. The pore was four layers in width. The $B-B$ interaction was set to $-3.3\,kT$, the $B-$surface interacton was $-1.1\,kT$, and all other interactions were set equal to zero. There is no external field in this calculation. (a) The spinodal points are marked by large dots, and the arrows represent the direction of integration. The dashed lines were added to guide the eye; no data was collected along them. It should also be noted that there is no data in the unphysical region of the isotherm. (b) The Gibbs integral construction for the phase coexistence data shown above. The coexistence line is obtained from the point where the lines cross (a bulk density of roughly 0.108 in this example). The dashed line comes from data in the unphysical region of the isotherm, which was approximated in this work as a linear function between the spinodal points.

the pore, the simulation box was filled initially to a density of 0.5 with a random mixture of molecules in the parallel and perpendicular orientations. At each move in the simulation, the program randomly selected one site in the lattice. The species on this site was then replaced with one of the three available species (holes, molecules in the parallel orientation, and molecules in the perpendicular orientation) according to the heat bath algorithm [40]. In this procedure, one first constructs energetic factors for each of the three species

$$f(\text{hole}) = 1$$

$$f(\text{parallel}) = \exp\left(\frac{\mu}{kT} - \frac{U_{\parallel}}{kT}\right)$$

$$f(\text{perpendicular}) = \exp\left(\frac{\mu}{kT} - \frac{U_{\perp}}{kT}\right)$$

Here, $U_{\parallel}$ and $U_{\perp}$ are the energies that molecules in the parallel or perpendicular orientation, respectively, experience when placed on the selected lattice site. Acceptance probabilities are then constructed by normalizing these energetic factors

$$p(\text{hole}) = \frac{f(\text{hole})}{f(\text{hole}) + f(\text{parallel}) + f(\text{perpendicular})}$$

$$p(\text{parallel}) = \frac{f(\text{parallel})}{f(\text{hole}) + f(\text{parallel}) + f(\text{perpendicular})}$$

$$p(\text{perpendicular}) = \frac{f(\text{perpendicular})}{f(\text{hole}) + f(\text{parallel}) + f(\text{perpendicular})}$$

A random number is generated between zero and one. If the random number is less than p(hole), the contents of the selected site are replaced with a hole. If the random number is between p(hole) and p(hole) + p(parallel), the contents of the selected site are replaced by a molecule in the parallel orientation. Otherwise, the contents of the lattice site are replaced with a molecule in the perpendicular orientation. Grand ensemble simulations for molecules in the bulk reservoir were run in a similar manner with the exception that periodic boundary conditions were used in all directions.

Each simulation run was allowed to equilibrate for one million Monte Carlo Steps (MCS), which are defined as one move for each site in the lattice. Thereafter, samples were taken at regular intervals for an additional nine million MCS. The average density, average energy per molecule, total system energy, and nearest neighbor probabilities were recorded. In cases where confined molecules were simulated, a snapshot of the molecule locations was obtained at the end of each run. Adsorption isotherms were constructed by comparing average densities from bulk and pore simulation runs at the same chemical potential.

Monte Carlo simulation runs were used to quantitatively verify the accuracy of the lattice DFT used in this work. Sample results of these tests for a pore ten lattice spaces in length and four lattice spaces in width are presented in Fig. 4. In Fig. 4a, the $B-B$ and $A-B$ molecule–molecule interactions were set equal to $-1.2\,kT$, the $B-$surface interaction was set equal to $-1.0\,kT$, and all other interactions were set equal to zero. In Fig. 4b, the $B-B$ and $B-$surface interactions were set equal to $-1.0\,kT$, and all other interactions were set equal to zero. The lines represent the parallel and perpendicular monomer densities in the layers directly adjacent to the walls, and the filled squares represent the Monte Carlo data. It can be seen from the figure that lattice DFT is in reasonable quantitative agreement with the Monte Carlo data.

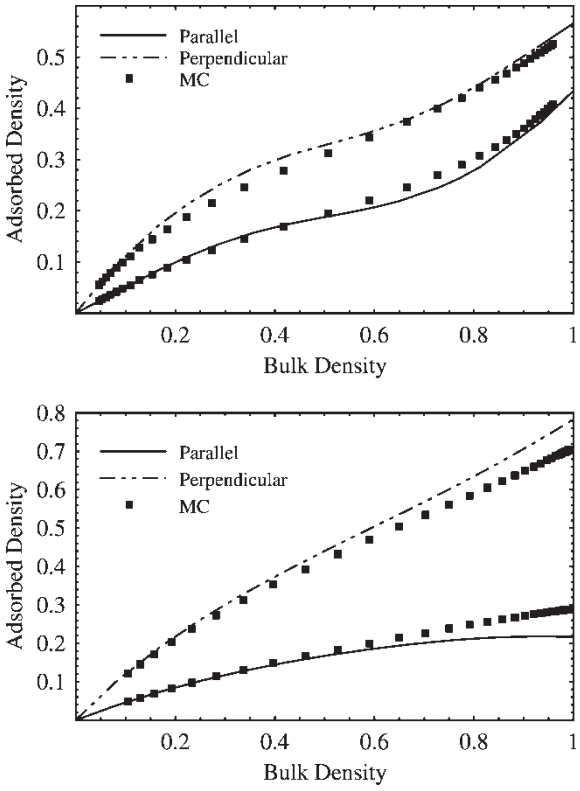

FIGURE 4 Lattice DFT calculations for first layer monomer densities are compared with grand ensemble Monte Carlo data for a pore ten layers in length and four layers in width. The first layer parallel and perpendicular monomer densities are represented by the solid and dashed lines, respectively, and the Monte carlo data is represented by the filled squares. The Monte Carlo data is in reasonable quantitative agreement with the theory. (a) The $B-B$ and $A-B$ molecule–molecule interactions are set to $-1.2\,kT$, the B–surface interaction is set to $-1.0\,kT$, and all other interactions are set equal to zero. (b) The $B-B$ and B–surface interactions are set to $-1.0\,kT$, and all other interactions are set equal to zero.

RESULTS AND DISCUSSION

Monomers with directional interactions confined within a pore have been discussed in a previous study [33]. In that work, it was shown that several types of phase transitions are possible, depending on the anisotropy of the molecular potentials. For sufficiently strong and anisotropic molecule–molecule interactions, it was found that chain formation could occur within the pore. The orientation of these chains could be controlled by specifying the molecule–surface interaction. The goal of the present work is to investigate the effect of an external field on adsorbed and confined molecules. It will be shown that an external field can be used to control chain orientation in the same manner as a strong molecule–surface interaction, with the added advantages that the field can be applied to a local section of a pore, and that it can easily be changed during the course of an experiment.

In this work, an external field is introduced that favors monomers in the perpendicular orientation. This effect is modeled after a classical dipole–field interaction. The dipole points in the direction of the B-sides of the monomer. If the monomer is in the perpendicular orientation, it is aligned with the field and there is a favorable interaction energy of $U = -\varepsilon_{\text{field}}(i)$. If the monomer is in the parallel orientation, the energetic contribution is zero. In this simple model, there is no case where the dipole is aligned against the field. The shape of this external field is shown in Fig. 2.

In order to simplify the parameter space in this study, the only non-zero molecule–molecule interaction is assumed to be $B-B$ nearest neighbor interaction. In all further discussion, the $A-A$ and $A-B$ interactions are set equal to zero. The pores considered in this study have four layers between their walls, and the adsorbed density is averaged over all four of these layers. However, the adsorbed density is considered explicitly as a function of layer number parallel to the walls (the i-direction, as shown in Fig. 2), so that the effect of the shape of the external field can be seen.

In Fig. 5a and b, the effect of the external field is shown on a pore with a length of ten lattice sites and a width of four lattice sites. Monomers in these calculations have a $B-B$ interaction of $-3.0\,kT$ and a B–surface interaction of $-1.0\,kT$. In Fig. 5a, there is no external field. As discussed previously [33], a local phase transition can be seen in the monomer density at a reservoir density of roughly 0.14. In Fig. 5b, the external field is turned on. The field has a maximum strength of $-1.0\,kT$, and a width of four lattice spaces. It can be seen that the phase transition in the central layers of the pore have shifted to lower bulk densities. In the center of the field (layers 5 and 6), the phase transition takes place at the lowest bulk density, roughly 0.045, while the next layers out (layers 4 and 7) undergo a phase transition at a density of roughly 0.06. The location of the phase transition in the layers outside of the field (layers 1–3 and 8–10) is unaffected. These results suggest that an external field can be used to control the bulk density at which a phase transition takes place. When molecule–surface interactions are strong, as in Fig. 5, the effect of the external field dies off quickly. This is evidenced by the fact that in layers 1 and 2 where the field is zero, the adsorption profiles overlap. Layer 3, which is also in a zero field region of the pore, is almost completely unaffected by the alignment of the neighboring monomers in layer 4. In contrast, if the molecule–surface interaction is very weak or not present, there is a much longer ranged correlation. As discussed earlier it becomes necessary to consider several layers out into the zero-field region of the pore before the adsorption profiles begin to overlap.

In order to probe the microstructure of the solution confined within the pores, Monte Carlo snapshots were obtained. The results of these simulations are

presented in Fig. 6. In order to more clearly show the formation of chains, the snapshots were taken for pores that were ten layers in width. Chain formation was also observed in Monte Carlo simulations of four-layer pores, although it can be more difficult to identify due to the small size of the pore. In Fig. 6, molecules have a B–B interaction of $-3.0\,kT$ and a B–surface interaction of $-1.0\,kT$. All other interactions are set equal to zero. Figure 6a is a Monte Carlo snapshot of a ten-layer pore with chemical potential set equal to $-3.6\,kT$. It can be seen that the molecules in the pore are relatively disordered. In Fig. 6b, the chemical potential has been increased to $-2.9\,kT$. The monomers have oriented themselves in the parallel conformation, and have formed chains that run parallel to the walls of the pore. These chains are the microstructure that results after the phase transition pictured in Fig. 5a. In Fig. 6c, the chemical potential has been set to $-3.2\,kT$, and an external field has been applied. The figure shows

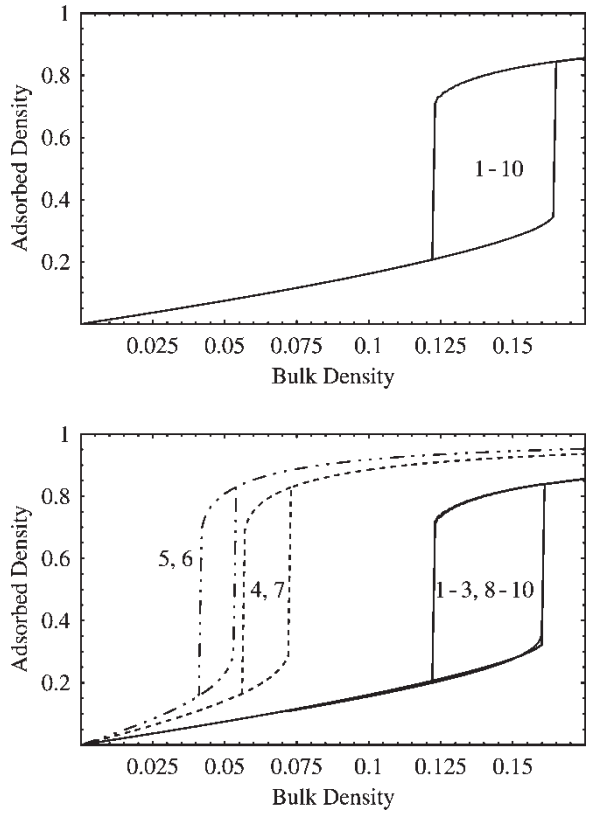

FIGURE 5 Data obtained in the phase coexistence region from lattice DFT by the method of successive substitutions for a pore four layers in width. The B–B interaction was set to $-3.0\,kT$, the B–surface interacton was $-1.0\,kT$, and all other interactions were set equal to zero. (a) Phase transition in the pore as a function of bulk density. There is no external field in this case. (b) Bulk density in the reservoir vs. local density in the pore with a locally applied external field. The field has a strength of $-1.0\,kT$ and has a shape as shown in Fig. 2. It can be seen that the layers in the pore under the influence of the external field undergo phase transitions at much lower bulk densities than those regions not under the influence of the field.

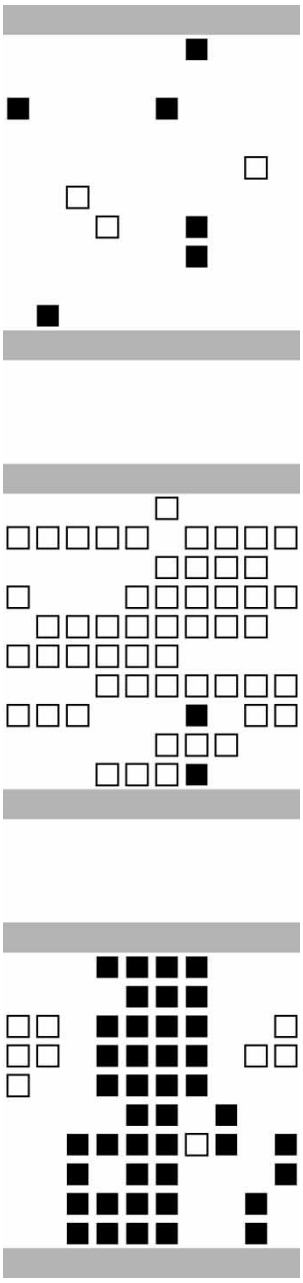

FIGURE 6 Snapshots taken from grand ensemble lattice Monte Carlo simulations for a pore ten layers in width. The monomers have a B–B interaction of $-3.0\,kT$, a B–surface interaction of $-1.0\,kT$, and all other interactions set equal to zero. The open and filled squares represent monomers in the parallel and perpendicular orientation, respectively. (a) Chemical potential is set equal to $-3.6\,kT$. It can be seen that the molecules are relatively unordered and sparsely packed. (b) Chemical potential is set equal to $-2.9\,kT$. Chains of molecules in the parallel orientation have formed and run in a direction parallel to the pore walls. (c) Chemical potential is set equal to $-3.2\,kT$, and an external field four layers in width is imposed. The field has a maximum strength of $-1.0\,kT$. In the region where the field is strongest, it can be seen that chains of monomers in the perpendicular orientation have formed, and they span the distance between the walls.

that molecules in the center of the pore form chains that span the distance between the walls, but long chains only occur in the region where the field is strongest. These chains are the dominant structure

after the phase transition shown in Fig. 5b. The reader should also note that in Fig. 6c, the chains of molecules that span the distance between the walls are in the perpendicular orientation.

It should be noted that Figs. 5 and 6 suggest that an external field can be used to induce a local phase transition in a local region of a pore at a lower bulk density than it would otherwise occur. If one were to introduce a pore into a solution with a bulk density of 0.1, there would be no phase coexistence in the pore. Upon the application of a local external field, the region of the pore inside the field would undergo a phase transition that both increases the adsorbed density in that region and also aligns the molecules.

The next set of figures show the effect of the external field on the phase transitions within the pore as a function of the overall molecular interaction strength. Three cases are compared according to the strength of the molecule–surface interaction; these are strong, weak, and intermediate values. In these figures, it should be noted that the molecule–molecule and molecule–surface interactions become weaker as the temperature is increased. For this reason, they are reported as ε/k in units of temperature, rather than the traditional ε in units of kT. In contrast, the molecule–field interaction does not change with temperature and remains fixed at $-1.0\,kT$. The binodal points for the phase transitions are obtained using the Gibbs integral construction, and are plotted as a function of temperature. This construction was done only within the strongest part of the field (layers 5 and 6). In addition, the phase diagrams are broken down into parallel, perpendicular and unordered components. The unordered component represents molecules with low orientational correlation. To better illustrate the nature of these components, an order–disorder phase transition is depicted in Fig. 7. The different components present during phase coexistence are labeled in the figure.

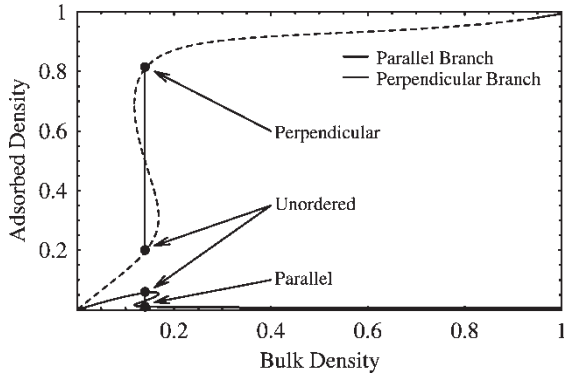

FIGURE 7 Parallel (solid line) and perpendicular (dashed line) components of an adsorption isotherm containing an order–disorder phase transition. During coexistence, three different phases are present in the system: a phase made up of molecules primarily in the parallel orientation, a phase made up of molecules primarily in the perpendicular orientation, and an unordered phase. The unordered phase is made up of molecules with low orientational correlation.

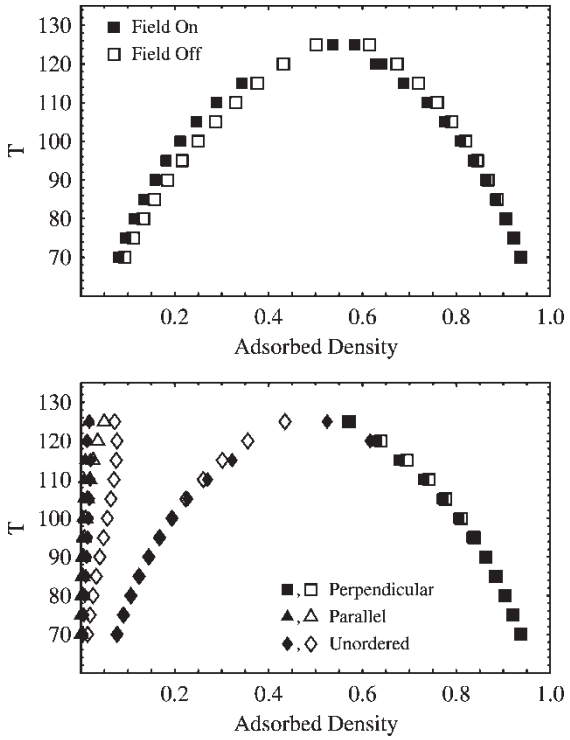

FIGURE 8 Plot of the overall layer five pore density at phase coexistence. The system has strong molecule–surface interactions and there are four layers between the walls of the pore. The B–B interaction is $-300\,K$, the B–surface interaction is $-150\,K$, and all other interactions are zero. As the temperature increases, these interactions get weaker. The local external field has a strength of $-1.0\,kT$ and does not change with temperature. (a) The field-off and field-on cases are represented by the empty and filled squares, respectively. It can be seen that the application of an external field has only a small effect on the location of the phase boundaries when the molecule–surface interaction is strong. (b) Densities of the parallel, perpendicular and unordered components at the phase transition. The perpendicular orientation for monomers is favored for both the field-on and field-off cases.

In Fig. 8, the effect of an external field on a system with a strong molecule–surface interaction is considered. The B–B and B–surface interactions are set to $-300\,K$ and $-150\,K$, respectively. All other intermolecular interactions are set equal to zero. The external field has an interaction strength of $-1.0\,kT$ and favors molecules in the perpendicular orientation. The strength of the external field does not change with increasing temperature. The empty symbols represent the case with the field off, while the filled symbols are for the case where the field is on. It can be seen in Fig. 8a that when the molecule–surface interaction is strong, the application of an external field has little effect upon the phase diagram for molecules within the pore. This observation suggests that the external field and the molecule–surface interaction have the same effect on the molecules; both favor chains in the perpendicular orientation after a phase transition has taken place.

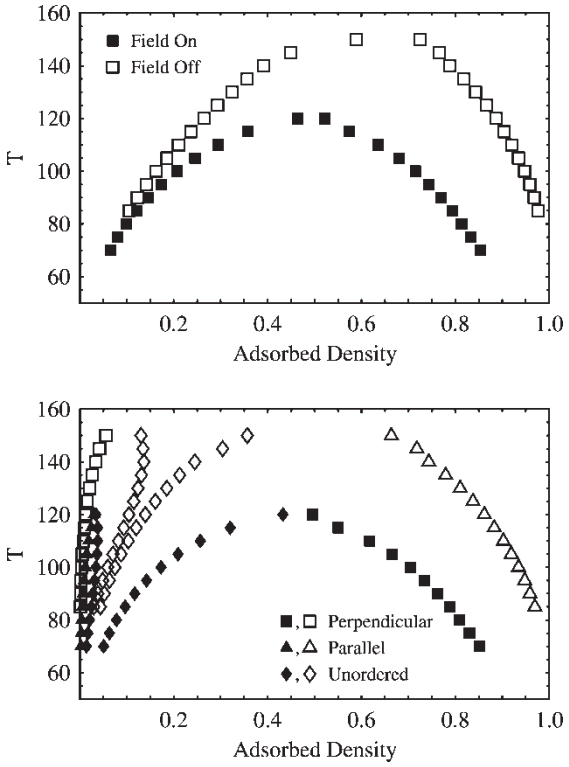

FIGURE 9 Plot of the overall layer five pore density at phase coexistence with no molecule–surface interaction. There are four layers between the walls of the pore. The B–B interaction is -300 K, and all other interactions are zero. As the temperature increases, these interactions get weaker. The local external field has a strength of -1.0 kT and does not change with temperature. (a) The field-off and field-on cases are represented by the empty and filled squares, respectively. When an external field is turned on, the phase transition is suppressed. This suggests that it is possible to disrupt a network structure in a local region of a pore by turning on an external field in that area. (b) Densities of the parallel, perpendicular and unordered components at the phase transition. In the absence of an external field, monomers in the parallel orientation are favored after the phase transition. In the presence of an external field, monomers prefer the perpendicular orientation. This is further discussed in the text.

Interestingly, the presence or absence of the external field does not affect the critical temperature for the phase transition, suggesting that the external field by itself cannot drive a phase transition. This is because increasing temperature makes the molecule–molecule and molecule–surface interactions weaker, but the strength of the external field remains constant at -1.0 kT and favors monomers in the perpendicular orientation. In order to get the monomers to form chains, it is necessary to have strong and anisotropic molecule–molecule interactions. A strong external field can only influence the orientation of the molecules after the phase transition. In Fig. 8b, the diagram is broken down into parallel, perpendicular and unordered components. Figure 8b shows that the perpendicular component is favored after a phase transition.

In Fig. 9, the molecule–surface interactions are set equal to zero. Only the B–B interaction is non-zero, which is fixed at -300 K. The external field has an interaction strength of -1.0 kT and favors molecules in the perpendicular orientation. The strength of the external field does not change with increasing temperature. In Fig. 9a, it can be seen that the application of an external field actually destabilizes the phase transition. When an external field is present, the region of the pore far from the field undergoes a phase transition. The region where the field is nonzero does not undergo a phase transition, although the overall density does increase very steeply. Interestingly, it can be seen that a strong external field has the same effect as a strong molecule–surface interaction. This is apparent by considering the field-on data (filled squares) in Fig. 9a and the field-off data (empty squares) in Fig. 8a.

In order to investigate the molecular mechanisms for the suppression of the phase transition, the adsorption of the individual components (parallel, perpendicular, and unordered) was studied. These results are presented in Fig. 9b. In the absence of an external field, it can be seen that the parallel orientation of monomers is favored. In the presence of an external field, perpendicular monomers are preferred. Grand ensemble Monte Carlo snapshots showing these types of ordering are presented in Fig. 10. In Fig. 10a, the temperature is 300 K. It can be seen that the monomers do not possess any long range order. In Fig. 10b, the temperature is dropped to 100 K. Monomers are seen to form chains parallel to the walls of the pore. In Fig. 10c, the temperature is further lowered to 75 K, and an external field is applied. It can be seen from the snapshot that the chains have switched their orientation and span the distance between the walls of the pore.

As evidenced by their differing critical temperatures in Fig. 9, chains oriented parallel to the walls are easier to form than chains oriented perpendicular to the walls, and the formation of perpendicularly oriented chains requires an additional input of energy, thus lowering the range of the phase transition. This effect could be exploited to break a chain-like network structure. To do this, a weak external field would need to be applied that opposes the direction of chain formation. This could be useful for breaking local ordering of molecules in a pore to allow for mixing. Upon application of a strong external field, the region of the pore under its effects can actually have a different network structure than the part of the pore that is not under the influence of the field.

In Fig. 11, a molecule–surface interaction of moderate strength is introduced. The B–B interaction is -300 K, the B–surface interaction is -70 K, and all other intermolecular interactions are set equal to zero. The external field has an interaction strength of -1.0 kT and favors molecules in the perpendicular orientation. The strength of the external field does

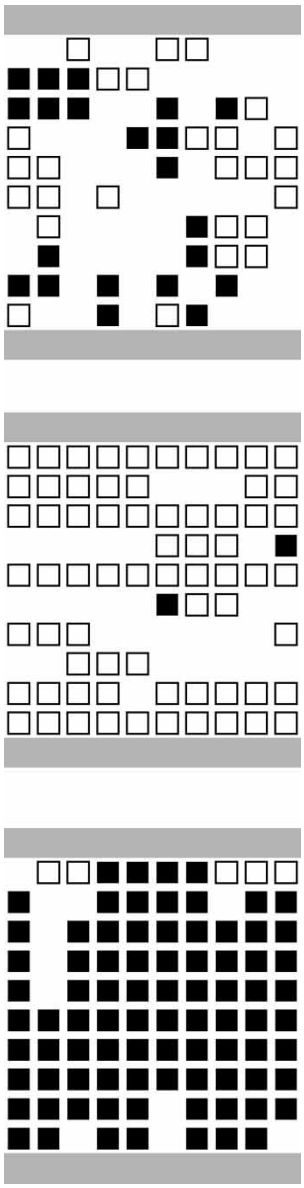

FIGURE 10 Snapshots taken from grand ensemble lattice Monte Carlo simulations for a pore ten layers in width. The open and filled squares represent monomers in the parallel and perpendicular orientation, respectively. The $B-B$ interaction is set to -300 K, and all other interactions are zero. (a) Temperature of 300 K, chemical potential of -1.0 kT, and no external field. (b) Temperature of 100 K, chemical potential of -2.7 kT, and no external field. (c) Temperature of 75 K, chemical potential of -2.7 kT, and an external field with a maximum strength of -1.0 kT.

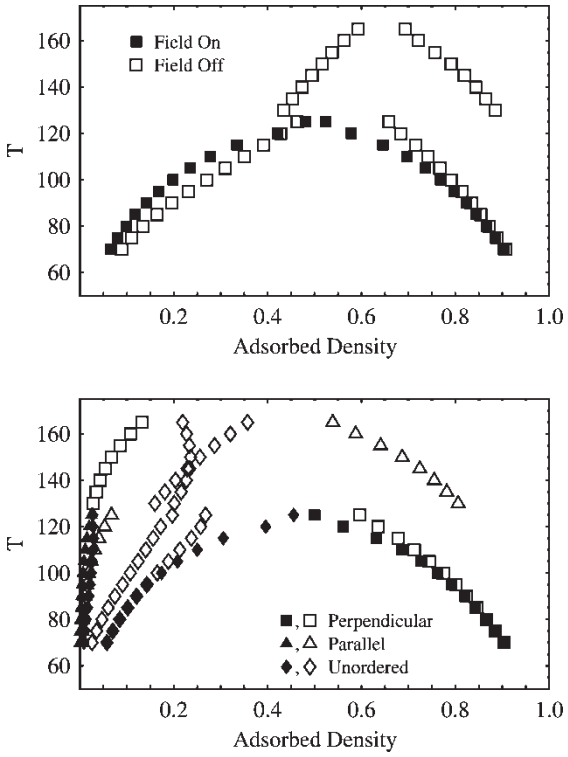

FIGURE 11 Plot of the overall layer five pore density at phase coexistence with no molecule–surface interaction. There are four layers between the walls of the pore. The $B-B$ interaction is -300 K, the $B-$surface interaction is -70 K, and all other interactions are zero. As the temperature increases, these interactions get weaker. The local external field has a strength of -1.0 kT and does not change with temperature. (a) The field-off and field-on cases are represented by the empty and filled squares, respectively. In the absence of an external field, the molecules can undergo one of two different phase transitions, depending on the temperature. In the presence of an external field, only one phase transition is observed. (b) Densities of the parallel, perpendicular and unordered components at the phase transition. In the absence of an external field, as the molecule-surface interaction gets stronger, the orientation of the molecules switches from parallel to perpendicular after a phase transition. When an external field is present, only molecules in the perpendicular orientation are observed after a phase transition.

not change with increasing temperature. In the case of no external field, Fig. 11a shows that the molecules in the pore can undergo one of two different phase transitions, depending on the temperature. However, when an external field is applied, only one phase transition is observed. In Fig. 11b, the parallel, perpendicular, and unordered components have been specified. In the case of no external field, parallel ordering is favored at high temperatures, but the ordering switches to the perpendicular orientation at lower temperatures. When an external field is applied, only perpendicular ordering occurs. In the case where the solution can form network structures oriented in different directions, these results show that it is possible to select between orientations by applying a local external field to the pore.

COMMENTS ON THE MEAN FIELD APPROACH

In this work, a mean field approach has been used to obtain adsorption isotherms and phase behavior of molecules with directional interactions. Mean field approaches are known to incorrectly predict the location of phase boundaries due to the absence of fluctuations in the theory. However, such approaches are of use because they can make correct qualitative predictions about the system of interest. Furthermore, mean field theories are a first step towards

a more accurate, quantitative approach. For example, it has recently been shown that (isotropic) lattice DFT can be used as the basis for a corrected theory that gives quantitative agreement within the critical region of the Ising phase diagram [42–44].

Despite the fact that mean field theories are not known for quantitatively accurate predictions, it is of interest to compare the interaction strengths and external field strengths used in this work to those found in real molecules. Many types of real molecules have directional interactions and can form the kind of network structures described in this work. As an example, hydrogen bonds are strongly directional and have measured interaction strengths of 0.5–40 kcal/mol [45], which translates to roughly 250–20,000 K/molecule. In this study, directional interactions as strong as 300 K are used, which translates to roughly 0.6 kcal/mol. These interactions are similar in strength to weak hydrogen bonds, such as those between H_2S molecules (measured at 1.1 kcal/mol), and are about one order of magnitude weaker than those found in water (measured at 5.0 kcal/mol), which is known to form network structures at room temperature.

Magnetorheological fluids are composed of micron-sized colloidal particles containing dispersed ferromagnetic materials with grain sizes of roughly 10 nm [11,46]. Since these grains have random orientations, the overall magnetization of the colloidal particles is completely reversible (termed "superparamagnetic"), and they can reversibly form network structures of long chains when exposed to a magnetic field. The required field strength for network formation can be tuned, and is a function of the (effective) magnetic susceptibility of the particles, the size of the particles, and the temperature. More specifically, network formation should not occur until the ratio of the maximum dipole–dipole interaction strength to the thermal energy kT is at least 1.0 [46]. Assuming a particle radius of 0.3 microns, a temperature of 300 K, and an effective magnetic susceptibility of 1.0 (these values are similar to measurements reported by Promislow and Gast [11]), obtaining a ratio of 1.0 requires an applied magnetic field of 0.591 kA/m (7.43 Oe). A ratio of 4.0 requires a magnetic field intensity of 1.18 kA/m (14.9 Oe). This work suggests that phase transitions into chains are possible at ratios of around 3.0.

CONCLUSIONS

In summary, a two-dimensional system of confined monomers with directional interactions on a square lattice has been studied both with and without the application of a local external field. It has been shown that the application of an external field can lower the reservoir density necessary for a phase transition to occur inside the pore. Furthermore, the external field can cause local ordering of monomers into network structures aligned with the field. In the case where the monomers interact strongly enough to form network structures in the absence of a field, a weak external field can sometimes be used to break the network, possibly to allow for mixing. If the molecules can form a second type of network structure, the locally applied field can be used to select this second microstructure over the first one. This control over the solution microstructure can be restricted to a local area inside the pore by applying the field to only a part of the porous region.

Acknowledgements

This work was supported by the Division of Chemical Sciences of the Office of Basic Energy Sciences, US Department of Energy under contract DE-FG0287ER13777.

References

[1] Stillinger, F.H. (1980) "Water revisited", *Science* **209**, 451.
[2] Angell, C.A. (1980) In: Franks, F., ed, *Water: A Comprehensive Treatise* (Plenum Press, New York), Vol. 7, pp 1–81.
[3] Stanley, H.E., Buldyrev, S.V., Canpolat, M., Havlin, S., Mishima, O., Sadr-Lahijany, M.R., Scala, A. and Starr, F.W. (1999) "The puzzle of liquid water: a very complex fluid", *Physica D* **133**, 453.
[4] Greer, S.C. (1995) "Living polymers", *Comp. Math. Sci.* **4**, 334.
[5] Greer, S.C. (2002) "Reversible polymerizations and aggregations", *Ann. Rev. Phys. Chem.* **53**, 173.
[6] Desai, A. and Mitchison, T.J. (1997) "Microtubule polymerization dynamics", *Ann. Rev. Cell Dev. Biol.* **13**, 83.
[7] Lauffer, M.A., Ansevin, A.T., Cartwright, T.E. and Brinton, C.C. (1958) "Polymerization–depolymerization of tobacco mosaic virus protein", *Nature* **181**, 1338.
[8] Bark, N., Foldes-Papp, Z. and Rigler, R. (1999) "The incipient stage in thrombin-induced fibrin polymerization detected by FCS at the single molecule level", *Biochem. Biophys. Res. Commun.* **260**, 35.
[9] Mosesson, M.W., Siebenlist, K.R. and Meh, D.A. (2001) "The structure and biological features of fibrinogen and fibrin", *Ann. N. Y. Acad. Sci.* **936**, 11.
[10] Rothlisberger, U. and Parrinello, M. (1997) "*Ab initio* molecular dynamics simulation of liquid hydrogen fluoride", *J. Chem. Phys.* **106**, 4658.
[11] Promislow, J.H.E. and Gast, A.P. (1996) "Magnetorheological fluid structure in a pulsed magnetic field", *Langmuir* **12**, 4095.
[12] Dolezalek, F. (1908) "Zur Theorie der Binären Gemische und Konzentrierten Lösungen", *Z. Phys. Chem.* **64**, 727.
[13] Muller, E.A. and Gubbins, K.E. (2001) "Molecular-based equations of state for associating fluids: a review of SAFT and related approaches", *Ind. Eng. Chem. Res.* **40**, 2193.
[14] Guggenheim, E.A. (1944) "Statistical thermodynamics of mixtures with non-zero energies of mixing", *Proc. R. Soc. London A* **183**, 213.
[15] Economou, I.G. and Donohue, M.D. (1991) "Chemical, quasi-chemical and perturbation theories for associating fluids", *AIChE J.* **37**, 1875.
[16] Wheeler, J.C. (1975) "Exactly soluble 2-component lattice solution with upper and lower critical solution temperatures", *J. Chem. Phys.* **62**, 433.
[17] Andersen, G.R. and Wheeler, J.C. (1978) "Directionality dependence of lattice models for solutions with closed-loop coexistence curves", *J. Chem. Phys.* **69**, 2082.

[18] Andersen, G.R. and Wheeler, J.C. (1978) "Theory of lower critical solution points in aqueous mixtures", *J. Chem. Phys.* **69**, 3403.
[19] Wheeler, J.C. and Andersen, G.R. (1980) "Some interesting new phase-diagrams in hydrogen-bonded liquid-mixtures", *J. Chem. Phys.* **73**, 5778.
[20] Davies, L.A., Jackson, G. and Rull, L.F. (2000) "Closed-loop phase equilibria of a symmetrical associating mixture of square-well molecules examined by Gibbs ensemble Monte Carlo simulation", *Phys. Rev. E* **61**, 2245.
[21] Visco, D.P. and Kofke, D.A. (1999) "A comparison of molecular-based models to determine vapor–liquid phase coexistence in hydrogen fluoride", *Fluid Phase Equil.* **158**, 37.
[22] Benjamin, I. (1999) "Structure, thermodynamics, and dynamics of the liquid/vapor interface of water/dimethylsulfoxide mixtures", *J. Chem. Phys.* **110**, 8070.
[23] Ikonomou, G.D. and Donohue, M.D. (1986) "Thermodynamics of hydrogen-bonded molecules—the associated perturbed anisotropic chain theory", *AIChE J.* **32**, 1716.
[24] Segura, C.J., Chapman, W.G. and Shukla, K.P. (1997) "Associating fluids with four bonding sites against a hard wall: density functional theory", *Mol. Phys.* **90**, 759.
[25] Tripathi, S. and Chapman, W.G. (2003) "Density-functional theory for polar fluids at functionalized surfaces. I. Fluid–Wall association", *J. Chem. Phys.* **119**, 12611.
[26] Aranovich, G.L. and Donohue, M.D. (1997) "New approximate solutions to the Ising problem in three dimensions", *Physica A* **242**, 409.
[27] van Pelt, A., Jin, G.X. and Sengers, J.V. (1994) "Critical scaling laws and a classical equation of state", *Int. J. Thermophys.* **15**, 687.
[28] Anisimov, M.A., Povodyrev, A.A., Kulikov, V.D. and Sengers, J.V. (1995) "Nature of crossover between Ising-like and mean-field critical behavior in fluids and fluid mixtures", *Phys. Rev. Lett.* **75**, 3146.
[29] Parola, A. and Reatto, L. (1995) "Liquid state theories and critical phenomena", *Adv. Phys.* **44**, 211.
[30] Choi, H.-Y., Harris, A.B. and Mele, E.J. (1989) "Mean-field theory for interchain orientational ordering of conjugated polymers", *Phys. Rev. B* **40**, 3766.
[31] Ispolatov, I. and Widom, B. (2000) "Unified approach to prewetting and wetting phase transitions", *Physica A* **279**, 203.
[32] Aranovich, G., Donohue, P. and Donohue, M. (1999) "A lattice model for fluids with directional interactions", *J. Chem. Phys.* **111**, 2050.
[33] Erickson, J.S., Aranovich, G.L. and Donohue, M.D. (2002) "A simple model for ordering in adsorbed layers", *Mol. Phys.* **100**, 2121.
[34] Aranovich, G.L. and Donohue, M.D. (2000) "Lattice density functional theory predictions of order–disorder phase transitions", *J. Chem. Phys.* **112**, 2361.
[35] Aranovich, G.L. and Donohue, M.D. (1999) "Phase loops in density-functional-theory calculations of adsorption in nanoscale pores", *Phys. Rev. E* **60**, 5552.
[36] Widom, B. (1996) "Theory of phase equilibrium", *J. Phys. Chem.* **100**, 13190.
[37] Boas, M.L. (1983) *Mathematical Methods in the Physical Sciences*, 2nd ed. (Wiley, New York), Chapter 4.
[38] Wu, D.-W., Aranovich, G.L. and Donohue, M.D. (2000) "Adsorption of amphiphilic dimers at surfaces", *J. Colloid Interface Sci.* **230**, 281.
[39] Ono, S. and Kondo, S. (1960) *Molecular Theory of Surface Tension in Liquids* (Elsevier, Amsterdam).
[40] Newman, M.E.J. and Barkema, G.T. (1999) *Monte Carlo Methods in Statistical Physics* (Clarendon Press, Oxford).
[41] Nicholson, D. and Parsonage, N.G. (1982) *Computer Simulation and the Statistical Mechanics of Adsorption* (Academic Press, London).
[42] Aranovich, G.L. and Donohue, M.D. (2003) "Critical point corrections for two- and three-dimensional systems", *Langmuir* **19**, 2162.
[43] Aranovich, G.L. and Donohue, M.D. (2003) "Theory of multilayer adsorption with correct critical behavior", *Langmuir* **19**, 3822.
[44] Aranovich, G.L. and Donohue, M.D. (2003) "Critical point corrections for lattice systems", *J. Chem. Phys.* **119**, 478.
[45] Desiraju, G.R. and Steiner, T. (1999) *The Weak Hydrogen Bond in Structural Chemistry and Biology* (Oxford University Press, Oxford), Chapter 1.
[46] Rosensweig, R.E. (1985) *Ferrohydrodynamics* (Cambridge University Press, Cambridge), Chapter 2.